EUROPEAN FUSION DEVELOPMENT AGREEMENT

EFDA-JET-CP(05)02-34

M.E. Puiatti, M. Valisa, C. Angioni, L. Carraro, I. Coffey, L. Garzotti,
P. Mantica, M. Mattioli, C. Sozzi and JET EFDA contributors

Analysis of Metallic Impurity Density Profiles in low Collisionality JET H-mode Plasmas

Analysis of Metallic Impurity Density Profiles in low Collisionality JET H-mode Plasmas

M.E. Puiatti[1], M. Valisa[1], C. Angioni[2], L. Carraro[1], I. Coffey[3], L. Garzotti[1], P. Mantica[4], M. Mattioli[1], C. Sozzi[4] and JET EFDA contributors[*]

[1]*Consorzio RFX - Associazione Euratom-Enea sulla Fusione, I-35127 Padova, Italy,*
[2]*Max Planck Institut fur Plasmaphysik, EURATOM-IPP Association, D-85748 Garching, Germany*
[3]*Department of Physics, Queen's University, Belfast, UK*
[4]*IFP- Istituto di Fisica del Plasma- CNR-EURATOM , 20125Milano, Italy*
** See annex of J. Pamela et al, "Overview of JET Results ",*
(Proc.20 th IAEA Fusion Energy Conference, Vilamoura, Portugal (2004).

Preprint of Paper to be submitted for publication in Proceedings of the
EPS Conference,
(Tarragona, Spain 27th June - 1st July 2005)

1. INTRODUCTION

A critical point in the determination of the ITER performance is to understand the behaviour of heavy impurity density profiles, in particular if in any plasma condition metallic impurity accumulation has to be expected, and how it can be controlled. In JET, heavy impurities have been found to behave differently in low collisionality H-mode discharges depending on the electron power deposition profiles and on the predominant RF heating channel. If RF heating is applied in Mode Conversion (MC, with ~20% ^{3}He) to heat electrons, Nickel density is found to be flat, while with ICRH in Minority Heating (MH, with ~8% ^{3}He, to heat ions) Nickel peaks. In this paper these results are presented and discussed within the ITG/EM stability theory. To analyse the impurity behaviour the technique of nickel Laser Blow Off (LBO) injection has been used.

2. THE EXPERIMENT

The discharges here analysed are H-modes where ≈3MW Ion Cyclotron RF Heating (ICRH) added on top of ≈12-14MW Neutral Beam Heating (NB) in MC (ICRH deposition radius $\rho_{ICRH} = 0.37$) or in MH (with $\rho_{ICRH} = 0.1$). All the discharges are at low collisionality, i.e. $0.1 \leq \nu_{eff} \leq 0.2$ at $\rho = 0.5$ ($\nu_{eff} = 10^{-14} \bullet n_e \bullet T_e^{-3} \bullet Z_{eff} \bullet R$, with n_e in m^{-3}, T_e in eV, R major radius in m). Despite the different electron power deposition profiles, the difference in the electron temperature profiles is modest (Fig.1). Electron density profiles are obtained as Single Value Decomposition inversions of the interferometric data (Fig.2). The simulation of the LBO pulses has been done by means of a 1D collisionalradiative impurity transport code [1] with the diffusion coefficient D and pinch velocity v as free parameters. A minimization procedure in the simulation of Ni spectral lines from different ion states and of the time evolution of Soft X-Rays (SXR) profiles has been adopted. Transient experiments as LBO allow the discrimination between the diffusion and convective terms in the transport equations. In the simulations reported in this paper, D and v do not need to be changed throughout the LBO pulse; moreover, the extrapolation to the steady state using the transport parameters deduced from the LBO analysis is well compatible with the SXR emission outside the pulse, when the contribution from the intrinsic carbon (from CX data) is also taken into account. This guarantees that the determined transport parameters are not perturbed by LBO itself.

3. RESULTS AND SIMULATIONS

The contour plots of SXR inverted emissivities during LBO reported in Fig.3 (where the profiles at $t = t_{LBO}$ have been subtracted) show a different Ni behaviour when ICRH is applied either in MH (left) or in MC (right): in the first case the penetration is slower, and Ni remains very peaked in the plasma centre for a much longer time. As a further evidence, Fig.4 shows that the brightnesses of spectral lines from low ionization stages, emitting from an external plasma region, have the same time evolution in MC and MH, while lines from the He-like ion, emitting in the core, exhibit shorter decay times in MC discharges, well distinguishable despite the low time resolution of the crystal spectrometer.

An example of simulation of the evolution of Ni SXR emissivity during LBO is given in Figs.5 and 6. The D and v profiles obtained as a result of the LBO simulations have been used to extrapolate the Ni density profile to the steady state (Fig.7). A strong peaking in the discharge with ICRH in MH is found, while in the example with ICRH in MC the Ni density is practically flat. Figure 8 shows for the two cases the diffusivity and pinch velocity compared with the neoclassical values (from NCLASS), together with the deuterium transport parameters and also with the heat diffusivity χ_e. Comparing the MH (red curves) and MC (blue curves) discharges, it appears that in the former (with Ni peaking) D_{Ni} is lower everywhere, in particular for $\rho < 0.2$, where it is close to the neoclassical value and much higher than the deuterium diffusion. The pinch velocity is inwards throughout the radius and much higher than the neoclassical. On the contrary, the MC shot shows an outward pinch, maximum around $\rho = 0.4$. A full comparison between D_{Ni}, D_D and χ_e is possible for the MC shots, where the perturbative transport analysis both of heat and of deuterium particle (from shallow pellet analysis) can be done. In this case, $D_{Ni} \approx \chi_e$ and $D_{Ni} \approx D_D$ is found; the central region at low diffusivity corresponds to the region below the critical threshold in the electron temperature gradient for the onset of ITG/TEM turbulence [2,3]. In the case of MH, only the effective $\chi_{e,\,PB}$ from power balance, as obtained from an interpretative simulation by the JETTO code [3] can be shown for comparison; the indication is that also $\chi_{e,\,PB}$ is about an order of magnitude higher than D_{Ni} in the plasma centre. For deuterium, in absence of shallow pellets, the determination of D and v is not fully independent. Despite this uncertainty, $D_D >> D_{Ni}$ for $\rho<0.2$ is found (consistently with a peaking factor higher for Ni than for D). In Figure 8 we report as an example the case with $D_D = 10\ D_{Ni}$ for $\rho<0.2$ and $D_D = D_{Ni}$ for $\rho>0.2$ and $v=0.5\ D\ \nabla q/q$, that allows a good reconstruction of the n_e profiles from SVD.

DISCUSSION AND CONCLUSIONS

The previous results have been interpreted using the linear gyrokinetic code GS2 [4] with two main species, deuterium ions and electrons, and a trace of Nickel, in extremely low concentration in order to be negligible in the quasineutrality condition. The calculations are electrostatic, and include the effects of collisions on all the species. From the linear relationship between nickel flux and nickel logarithmic density gradient, the nickel diffusion coefficient and pinch velocity can be determined. The couples of parameters [R/L_{ne}, R/L_{Te}], [R/L_{ne}, Te/Ti] and [R/L_{ne}, R/L_{Ti}] have been scanned over intervals largely covering the experimental variations in the considered discharges (R = major radius, $L_{ne} = n_e/\nabla n_e$, $L_{Te} = T_e/\nabla T_e$, $L_{Ti} = T_i/\nabla T_i$). The result is summarised in Fig.9, showing the Ni peaking factor (R ßv/Dß) at different values of R/L_{ne} (from 1 to 6) as a function of R/L_{Te} and T_e/T_i. As electron density gradient increases, the Ni peaking factor decreases: this anomalous effect is opposite to the usual neoclassical behaviour. Also the increase of T_e/T_i has the effect of flattening the impurity density profile; large values of T_e/T_i imply flat impurity profiles for any value of R/L_{ne}, due to large values of the Ni diffusion and reduced values of the anomalous pinch. Figure 9 shows that, despite the modest experimental variations of electron density and temperature profiles, the experimental findings are in qualitative agreement with these scalings.

Concerning the dominant modes, the theoretical prediction is that ITG modes, associated to a rotation in the ion drift direction (positive), correspond to an inward thermodiffusion, while TEM modes, associated to a rotation in the electron drift direction (negative), correspond to an outward thermodiffusion [5]. The simulation referring to two of the shots analysed in this paper, one in MH and the other in MC is shown in Fig.10. In the discharge in MC (flat Ni profiles) the drift velocity is negative (TEM) for $\rho \geq 0.4$, but not for $\rho < 0.3$, where Ni accumulation occurs. However, this is compatible with the experimental Ni behaviour, observing that just around $\rho = 0.4$ we find the region of high gradient of D, that decreases to quasi-neoclassical values in the MH shots; moreover, calculations with the impurity transport code show that an outward term in the flux localized around the middle of the plasma radius can result in a flattening of Ni profile in the centre. Indeed, just around $\rho = 0.4$ the outward pinch found for the MC shots is higher.

Summarizing, the flat Ni profile in low collisionality JET discharges with RF power to electrons deposited at mid-radius is the result of two phenomena: on the one hand an on-axis diffusivity higher than in the MH shots, and on the other hand an outward component of the flux and a lower gradient of the diffusion in the mid-radius region. GS2 analysis including trace Ni predicts that TEM instabilities, present in MC shots, introduce an outward Ni flux. Ad hoc experiments are planned on JET to further investigate the importance of the shape of the electron power deposition profile as a tool to control the heavy impurity profiles and its relevance to ITER

ACKNOWLEDGEMENT

This work, supported by the European Communities under the contract of Association between EURATOM/ENEA, was carried out within the framework of the European Fusion Development Agreement. The views and opinions expressed herein do not necessarily reflect those of the European Commission.

REFERENCES

[1]. M. Mattioli et al., J. of Phys. B **34** (2001) 127

[2]. M.E. Puiatti et al., 31st EPS Conf. on Plasma Phys., London, (2004) ECA Vol. **28G**, paper P-1.151

[3]. X. Garbet et al., Plasma Phys. Contr. Fusion **46** (2004) 1351

[4]. Cenacchi G. Taroni A, Report ENEA-RT-T113-88-5

[5]. C. Angioni et al.,'Gyrokinetic calculations of particle transport in AUG and JET', this conference,P4.041

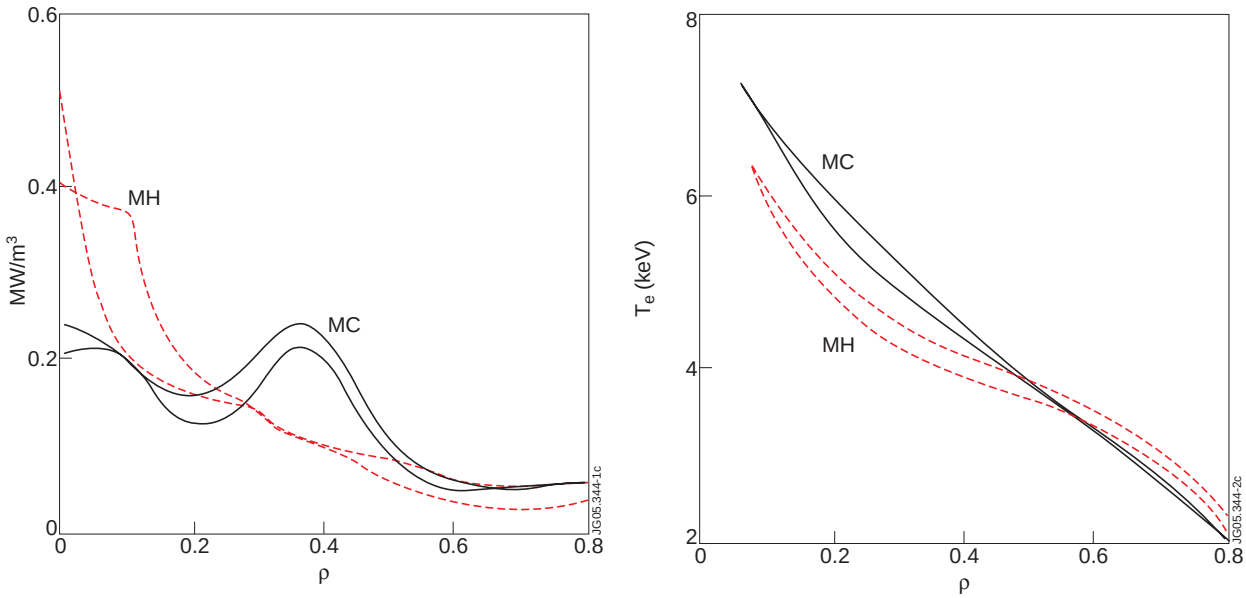

Figure 1: electron power deposition and temperature profiles in MH (red) and MC (blue) shots: The electron power includes both RF and NB power.

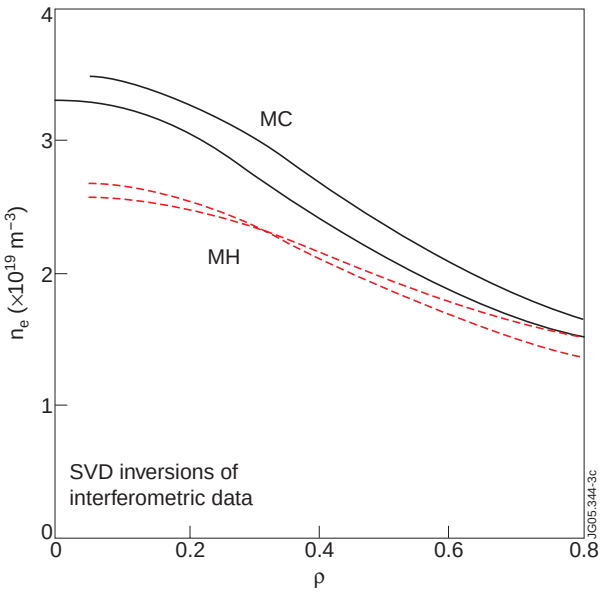

Figure 2: electron density profiles from SVD inversions of interferometric data.

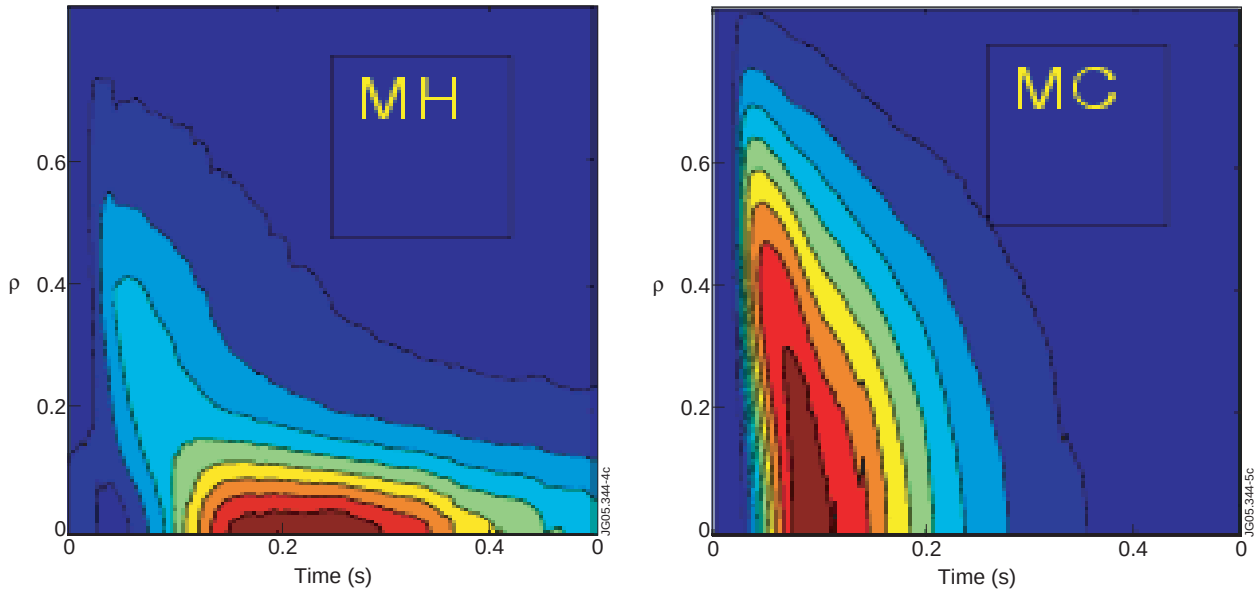

Figure 3: inverted SXR emissivities in MH (left) and MC (right) shots.

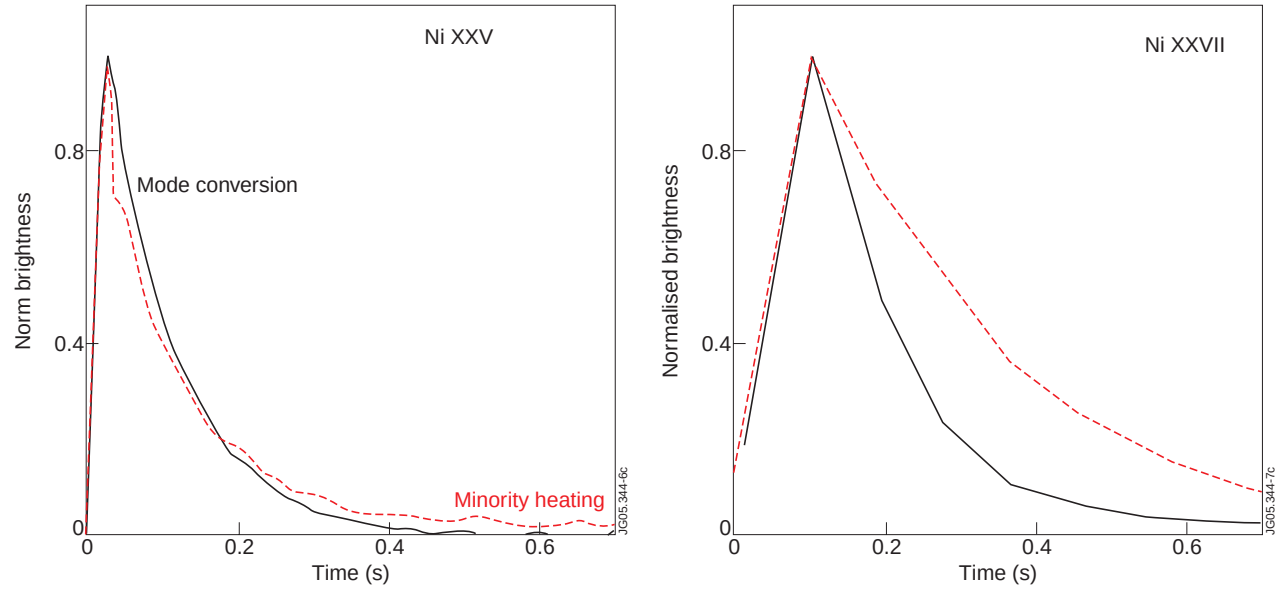

Figure 4:evolution of Ni line brigthnesses in MH and MC discharges.

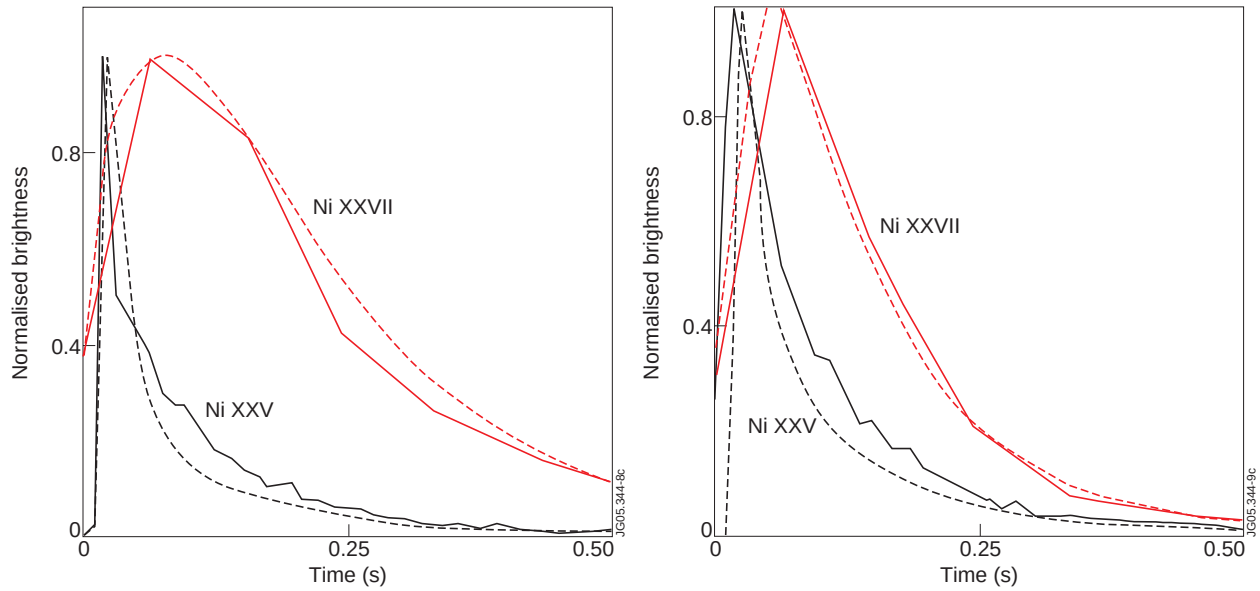

Figure 5: simulation of the evolution of Ni spectral lines.

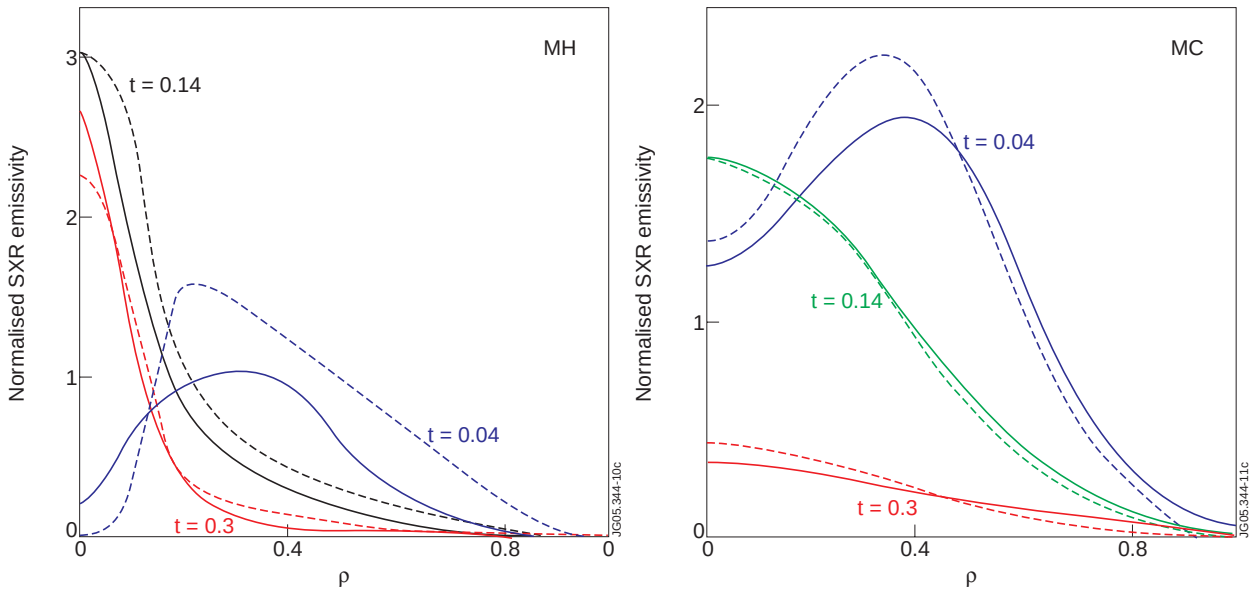

Figure 6: simulation of SXR emissivity profiles in MH and MC shots.

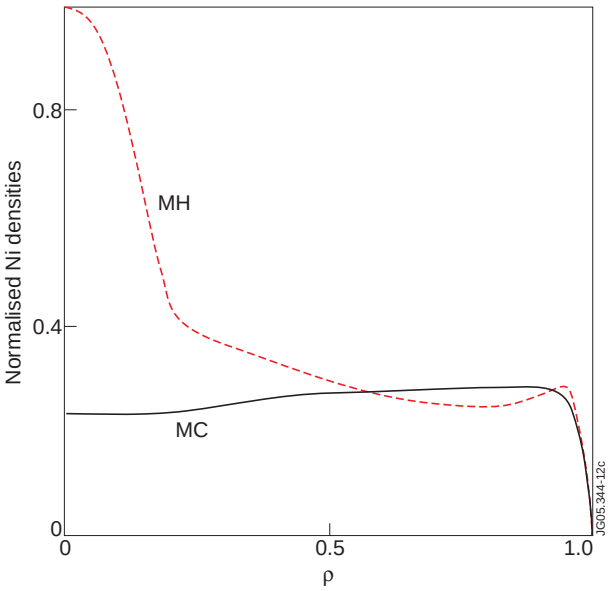

Figure 7: Ni density profiles at the steady state.

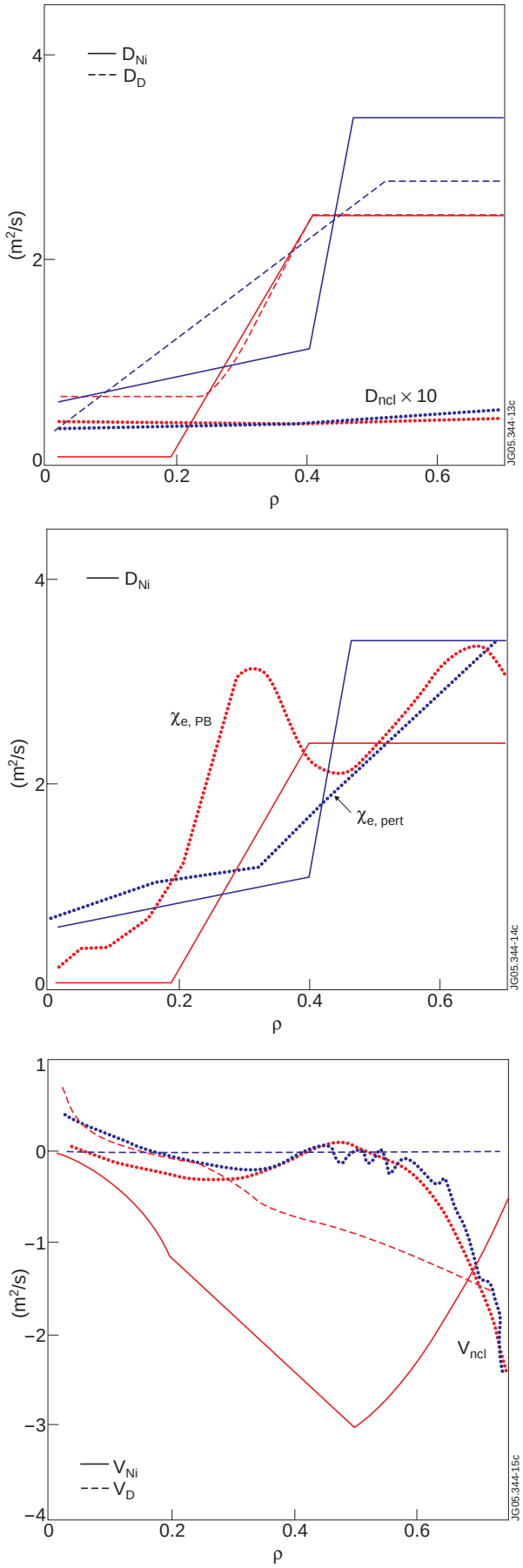

Figure 8: Ni D compared with deuterium and neoclassical (left) and heat diffusivities (centre). Right: Ni, deuterium and neoclassical pinch velocities.

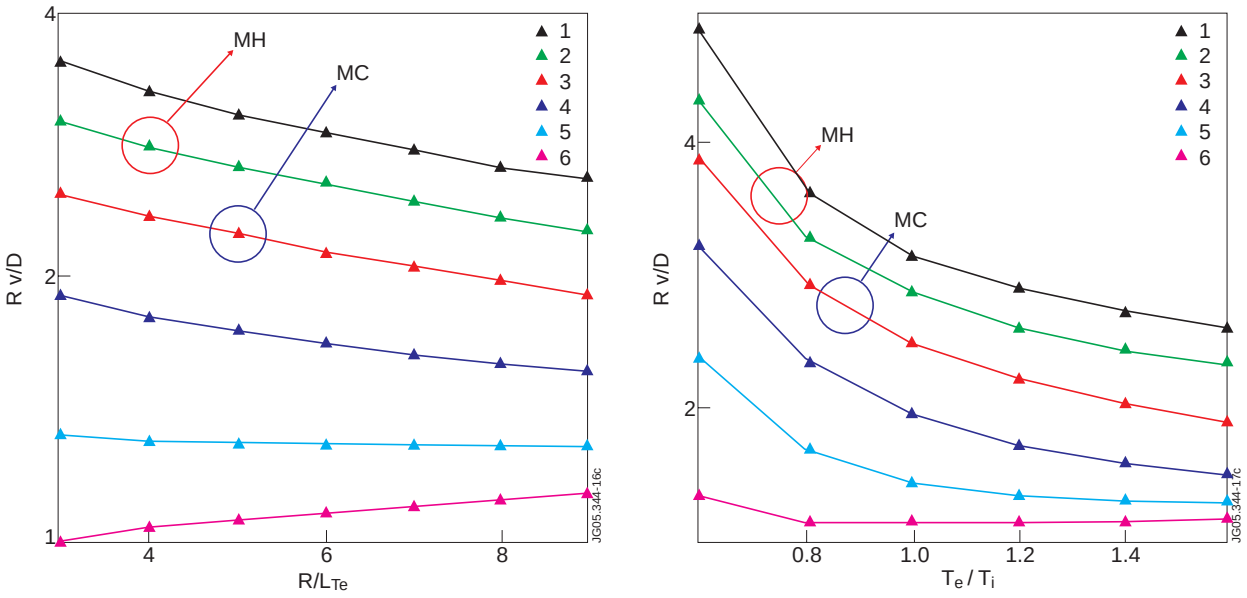

Figure 9: Scaling of Ni peaking factor with R/L_{Te} and Te/Ti for different R/L_{ne} (from 1 to 6).

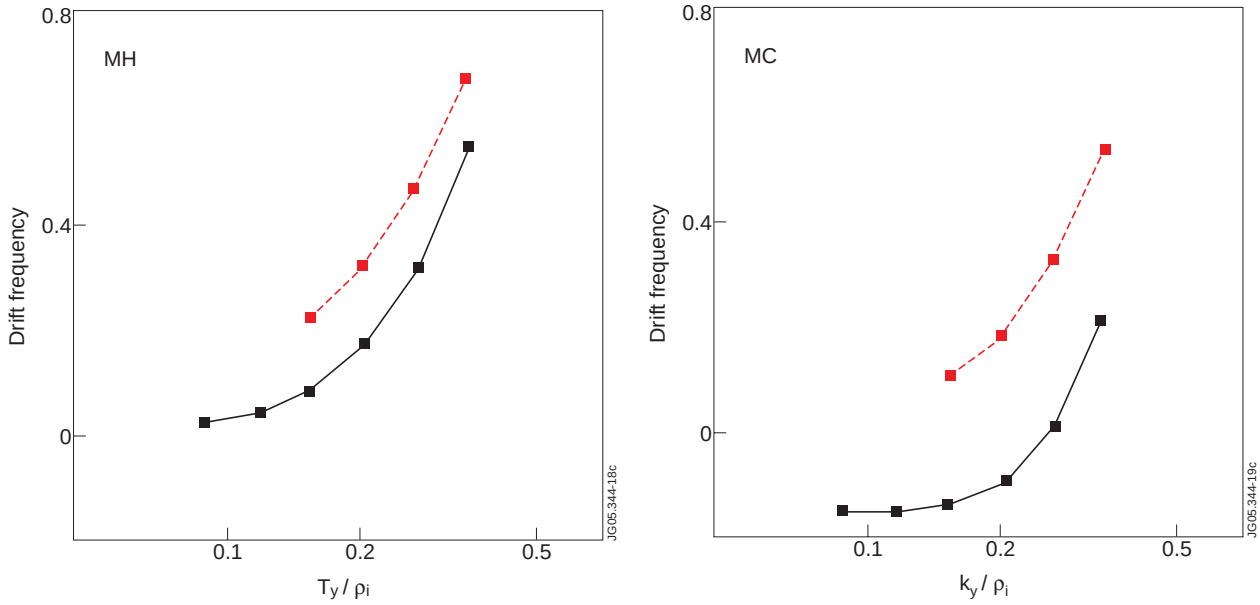

Figure 10: drift frequency from GS2. Red: ρ = 0.3; blue: ρ = 0.5.